

Mitigating the Effect of Nanoscale Porosity on Thermoelectric Power Factor of Si

S. Aria Hosseini¹, Giuseppe Romano², P. Alex Greaney^{1,3*}

¹Department of Mechanical Engineering, UC Riverside, Riverside CA 92521

²Department of Mechanical Engineering, Massachusetts Institute of Technology, Cambridge Massachusetts 02139

³Materials Science and Engineering Program, UC Riverside, Riverside CA 92521

*Corresponding author: greaney@ucr.edu

The addition of porosity to thermoelectric materials can significantly increase the figure of merit, ZT, by reducing the thermal conductivity. However, porosity also is detrimental to the thermoelectric power factor in the numerator of ZT. In this manuscript we derive strategies to recoup electrical performance in nanoporous Si by fine tuning the carrier concentration and through judicious design of the of pore size and shape so as to provide energy selective electron filtering. A semiclassical Boltzmann transport equation is used to model Si thermoelectric power factor. This model reveals three key results: The largest enhancement in Seebeck coefficient happens for cubic pores with characteristic length around 0.85 nm. For the best energy filtering threshold, nanoporous Si is needed to be doped to higher carrier concentration compared to bulk Si. We show that in a n-type thermoelectric the highest practical filtering threshold that can be provided by a dispersion of spherical nanopores with characteristic length around 16 nm giving a theoretical maximum power factor as high as 89% of the maximum power factor that can be obtained in bulk Si at room temperature.

KEYWORDS: bulk thermoelectric, electron transport, nanoporous, electron filtering.

I. INTRODUCTION

In the quest to create inexpensive thermoelectric (TE) materials that can be used for harvesting low grade waste heat, researchers have identified the strategy for improving thermoelectric

performance in materials such as Si by engineering nanoscale porosity.^{1,2} Nanoscale pores with a spacing smaller than the typical phonon mean free path hinder heat transfer by phonons and can produce a dramatic reduction in thermal conductivity.³ However, although the electron mean free path is much smaller than the phonon mean free path, porosity damages the electron transport properties. In this manuscript we examine strategies for designing porosity to minimize their damage to the electronic contribution to thermoelectric performance. Our approach to mitigate the effect of pores is to identify conditions in which reduction in electrical conductivity due to scattering from pores is offset by improvement of the Seebeck coefficient achieved by electron filtering.

The performance of thermoelectric materials at a given temperature, T , is quantified by the dimensionless figure of merit, $ZT = \frac{\sigma S^2}{\kappa_e + \kappa_l} T$, where σ is electrical conductivity, S is Seebeck coefficient, κ_e and κ_l are electron and lattices thermal conductivity, respectively.⁴ The TE figure of merit depends on a combination of strongly interdependent electrical transport properties, that have countervailing dependence of the carrier concentration so that the overall scope for enhancing the power factor is limited. The tradeoff of these parameters is well studied, and it has become an accepted truth that optimal performance of bulk TE can be obtained in semiconductors that are highly doped to a narrow window of optimized charge carrier concentration.⁴

The electrical transport properties that appear in ZT can be derived from the semiclassical Boltzmann transport equation using the single relaxation time approximation.⁵ In this model, the electrical conductivity, σ , is written as

$$\sigma = -\frac{1}{3} e^2 \int \chi(E, T) \tau(E, T) dE, \quad (1)$$

where e is electron charge, $\tau(E, T)$ is momentum relaxation time of electrons with energy E at temperature T in n -doped semiconductors. The kernel χ includes all the intrinsic non-scattering terms and is given by

$$\chi(E, T) = v(E)^2 \frac{\partial f(E_f, E, T)}{\partial E} D(E), \quad (2)$$

Here E_f is the Fermi level, $v(E)$ the carrier group velocity, $f(E_f, E, T)$ the Fermi-Dirac distribution, and $D(E)$ is density of states available for charge carriers. The Seebeck coefficient, S , in ZT describes the diffusion of electrons due to temperature gradient and is related to the difference

between the average energy at which current flows and the Fermi energy level.⁶ In bulk material, with negative charge carrier, the Seebeck coefficient is given as⁷

$$S = \left(-\frac{k_B}{e} \right) \left(\frac{E_c - E_f}{k_B T} + \delta \right), \quad (3)$$

where k_B , E_c are Boltzmann constant and conduction band edge, respectively. The dimensionless parameter δ is a describes how far the average energy of the current carrying charge flow is from the conduction band edge. It is defined as $\delta = \frac{\Delta_1}{k_B T}$, where $\Delta_1 = E_\sigma - E_c$, and E_σ is the average energy of the charge carrier weighted by their contribution to electrical conductivity

$$\Delta_n = \frac{\int \chi(E, T) \tau(E, T) E^n dE}{\int \chi(E, T) \tau(E, T) dE}. \quad (4)$$

The central concept of energy filtering is to provide sources of scattering that selectively impede low energy electrons so as to increase Δ by reshaping product $\chi(E, T) \tau(E, T)$ so that it is more strongly asymmetric about the fermi energy.

II. ELECTRON TRANSPORT IN NANOPOROUS SILICON

Nanoporous materials are among the prime candidates for electron filtering. The band bending at the interface of pores presents a large potential energy barrier to electron transport with height, U_o , equal to the semiconductor's electron affinity.⁴ This potential impedes transport of the low energy electrons while presenting little extra resistance to electrons in high energy states.

A. Extrinsic electron-pore scattering rate

This scattering, which occurs in addition to the intrinsic scattering from phonons and impurities, changes the electron lifetime by introducing a perturbation potential that for a single pore can be described as $U = U_o \Pi(\mathbf{r})$, where, $\Pi(\mathbf{r})$ is a dimensionless boxcar function equal to unity inside the pore and zero outside of it. For uniform distribution of pores, the electron momentum relaxation time is defined as⁴

$$\tau_{np}^{-1}(s) = \frac{N}{8\pi^3} \int SR_{kk'} (1 - \cos\theta) d\mathbf{k}', \quad (5)$$

where N , is the number density of pores. This is related to porosity through $N = \varphi/V_{pore}$, where φ is the porosity and V_{pore} is the volume of the pores. The term $SR_{kk'}$ in equation (5) is the probability of transition from an initial state with wave vector k and energy E to a state k' with

energy E' . The $(1 - \cos\theta)$ term accounts for the change in momentum that accompanies this transition, with θ the angle between initial and scattered wavevectors. For a time-invariant potential, the transition rate $SR_{kk'}$ is given by Fermi's golden rule^{4,8}, $SR_{kk'} = \frac{2\pi}{\hbar} (M_{kk'} \bar{M}_{kk'}) \delta(E' - E)$. In this expression $M_{kk'}$ is the matrix element operator that describes the strength of the coupling between initial and final states and the number of ways the transmission happens. For the Bloch waves, $M_{kk'}$ is defined as

$$M_{kk'} = \int e^{i(k'-k)\cdot r} U(\mathbf{r}) d\mathbf{r}. \quad (6)$$

For energy conservative (elastic) electron-pore scattering only transmission to eigenstates with the same energy level is possible so the Brillouin zone integral in equation (5) can be written as a surface integral over the isoenergetic k space contour:

$$\tau_{\text{np}}^{-1}(\text{s}) = \frac{N}{4\pi^2 \hbar} \oint_{E(\mathbf{k}')=E(\mathbf{k})} \frac{M_{\mathbf{k}\mathbf{k}'} \bar{M}_{\mathbf{k}\mathbf{k}'}}{|\nabla E(\mathbf{k}')|} (1 - \cos\theta) dS(\mathbf{k}'), \quad (7)$$

where $S(\mathbf{k}')$ is the electron isoenergy state for a given wavevector. In most semiconductors isoenergy states close to the conduction valley have ellipsoid shape in momentum space that can be approximated as $E(\mathbf{k}) = \frac{\hbar^2}{2} \left[\frac{(k_x - k_{ox})^2}{m_x^*} + \frac{(k_y - k_{oy})^2}{m_y^*} + \frac{(k_z - k_{oz})^2}{m_z^*} \right]$, where $E(\mathbf{k})$, $\mathbf{k}_o = (k_{ox}, k_{oy}, k_{oz})$, m_x^* , m_y^* , m_z^* are energy level from conduction band edge, conduction band minimum, effective masses along k_x , k_y and k_z , respectively.

In this study, we considered nanoporous phosphorous doped silicon containing one of four different shaped pores: spheres, cylinders, cubes, and triangular prisms, which are shown in the inset in the right-hand plot of figure (1). The spherical pore has radius r_o , the edges of the cube are length l_o , the cylinder has radius r_o and height $2r_o$ and all the edges of the triangular prism are l_o . The characteristic length (volume to surface area ratio) of these shapes are $\frac{1}{3}r_o$, $\frac{1}{6}l_o$, $\frac{1}{3}r_o$ and $\frac{1}{2+4\sqrt{3}}l_o$, respectively. The analytic expression for the scattering matrix element, $M_{kk'}$ for each pore shape is presented in section B of the APPENDIX. In spite of the poor thermoelectric efficiency of bulk silicon due to its high thermal conductivity, it provides an excellent platform for studying the role of design parameters on transport properties, since its bulk properties are

extremely well characterized.^{9,10,11} We have validated the transport model against a set of phosphorous-doped Si based thermoelectrics.¹²

The terms $D(E)$, and $v(E)$, in function χ for Si were derived from the conduction band of Si computed with density functional theory (DFT). The calculations are described in detail in section A of the APPENDIX. The final material property that appears in function χ is the Fermi level. In P-doped silicon this depends strongly on the carrier concentration, which varies non-monotonically with temperature as the solubility of the dopant changes. We used a self-consistent approach to compute E_f by setting the conduction band edge as the reference frame and computing E_f that gives the same carrier population in DFT computed band as the carrier population calculated experimentally.

B. Intrinsic electron scattering rate in bulk silicon

To complete the transport model, we need to define the electron lifetime, $\tau(E, T)$ in bulk Si — that is the coherence time of electrons between intrinsic scattering events in bulk Si containing no pores. At high temperatures, this scattering is predominated by electron-phonon interactions which we have previously modeled as a power law in electron energy and temperature,⁶ $\tau_p(E) = \frac{A_o}{\sqrt{ET}}$. The coefficient A_o was tuned to a value of 220.5 fs.(eV.K)^{1/2} to fit the electrical conductivity measured experimentally in P-doped Si whose synthesis and characterization are described in ¹². For the Seebeck coefficient, A_o , the model's single tuning parameter, cancels from the numerator and denominator of equation (4) giving a parameterless prediction for S . A plot of this fit is given in the APPENDIX which shows that the model gives a good match to the experimental σ and S across the full range of measurement temperatures. The calculations were performed used a python package, *thermoelectric.py*, that we have made available for download through GitHub¹³.

We assume that electron-pore scattering is independent of the electron-phonon scattering and thus Matthiessen rule can be used to sum the scattering rate from the two processes giving total scattering rate, $\tau^{-1} = \tau_p^{-1} + \tau_{np}^{-1}$.

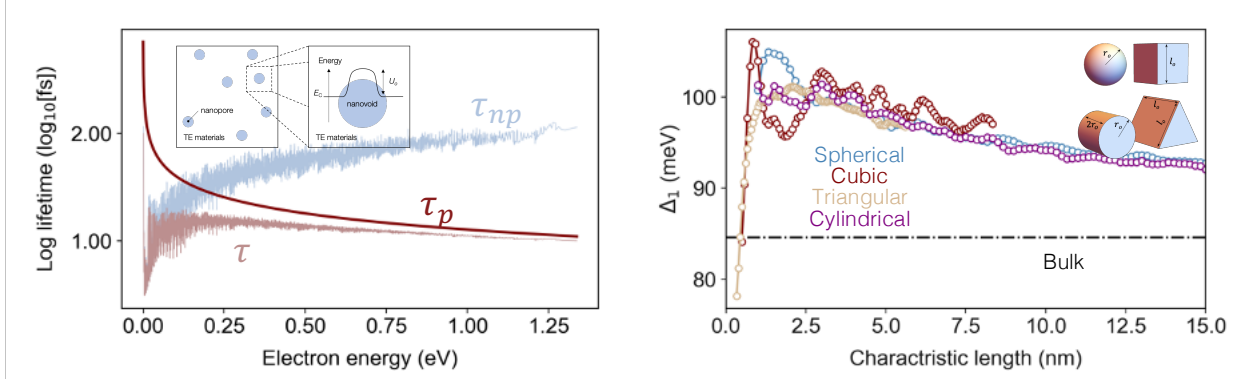


Figure 1: (left) Electron lifetime due to phonon (red) and pore (blue) scattering for 0.05 porosity at 300K and total lifetime (brown). Electron-pore scattering is dominant for electron with energy less than 22 meV. The average energy of charge flow increased about 15.1 meV by introducing pores. This increases the Seebeck coefficient by 18%. (right) The variation of average energy of electron vs effective length for pores with different shapes but fixed porosity of $\phi = 0.05$. The four geometries examined in this work and their characteristic lengths in parenthesis. Clockwise from the top left: sphere ($l_c = \frac{1}{3}r_o$), cube ($l_c = \frac{1}{6}l_o$), triangular prism ($l_c = \frac{1}{2+4\sqrt{3}}l_o$), and cylinder ($l_c = \frac{1}{3}r_o$).

C. Seebeck enhancement due to electron energy filtering by pores

Silicon's conduction band minimum is located at $k_o = \frac{2\pi}{a}(0.85,0,0)$, where a is the lattice parameter equal to 5.43 Å, and $m_x^* = 0.98 m_o$, $m_y^* = m_z^* = 0.19 m_o$ where m_o is electron rest mass equal to 9.11×10^{-31} kg.¹¹ The left-hand plot in figure (1) shows the scattering lifetimes for intrinsic electron-phonon and extrinsic electron-pore scattering computed in P-doped Si containing 5% porosity due to 10 nm spherical pores at 300 K. The noise in the lifetime reflects the difference in scattering rate of wavevectors around the valley minimum. Pores are the dominant scattering term for electrons with energy less than 220 meV. For a carrier concentration of 6.3×10^{19} cm⁻³, the average energy of charge carrier in the bulk P-doped Si is $\Delta_1 = 84.6$ meV while in the nanoporous Si $\Delta = 99.7$ meV. This 18% enhancement in Δ_1 of the nanoporous Si is due to the electron filtering.

Introducing pores into Si will not change the concentration of carrier concentration locally in the remaining Si (nor the Fermi energy), but it will change the volume averaged carrier concentration due to the reduction in the volume averaged density of states. This will impact the conductivity, and thus the effective electrical conductivity of porous materials is modeled as $\sigma_{\text{eff}} = (1 - \phi)\sigma_{np}$. This change does not affect the Seebeck coefficient since the changes in density of state cancels out for the denominator and numerator of S equation. We assumed that pores do not change the band structure of the Si. This is a reasonable assumption for low porosity, so we limit our study

to the pores taking up 5% volume fraction — a level that is still sufficient to reduce the thermal conductivity of Si by an order of magnitude.³

D. Maximum enhancement in power factor

The maximum power factor ($PF = \sigma S^2$) in P-doped bulk Si at 300 K occurs at carrier concentration $6.3 \times 10^{19} \text{ cm}^{-3}$ which has the $E_f = 41.8 \text{ meV}$ above the conduction band minimum. The right-hand plot in figure (1) shows Δ , the average energy of the current carrying electrons, as a function pore size. In bulk Si, Δ_1 is 84.6 meV. The cubic pores provide the largest Δ enhancement ($\Delta_1 = 106.0 \text{ meV}$) following by spherical pores ($\Delta_1 = 104.9 \text{ meV}$). These correspond to 25.3% and 23.9% enhancement in Seebeck coefficient, respectively, with the optimal characteristic length of the pores being 0.83 nm and 1.3 nm. However, the key message from the plot of Δ_1 in figure (1) is that there is only little additional return on the effort required to make pores have particular geometry—most of the benefit comes from making the pores small. This means that as a design strategy for thermopower enhancement one should seek to create pores of any shape, but to make them as small as possible. We note that the largest enhancement in S does not necessarily provide the maximum power factor. For the best PF performance, the countervailing response of enhancement in S and reduction in σ should be considered simultaneously.

The left-hand panel in figure (2) shows the model prediction for the variation in TE power factor with carrier concentration in nanoporous Si at 300 K. The power factor in bulk Si is marked in open circle. In the narrow carrier concentration window with the highest PF, bulk Si always shows better performance. The large energy difference between the conduction band edge in the Si and the vacuum level in the pore (about 4.15 eV electron affinity of bulk Si¹⁴) causes significant electron scattering. This reduces the electrical conductivity more than enough to offset the benefit of the enhanced Seebeck coefficient in the PF and leads to an overall reduction in performance. However, much of the reduction in PF can be recuperated by tuning the dopant level to increase the carrier concentration.

Pores significantly lower the electrical conductivity, therefore the filtering effect (enhancement of S) in nanoporous Si cannot lead to power factor higher than bulk Si; however, engineering the electron selective scattering can mitigate the degradation of PF. The maximum PF in porous structures takes place at carrier concentrations higher than the optimal carrier concentration in

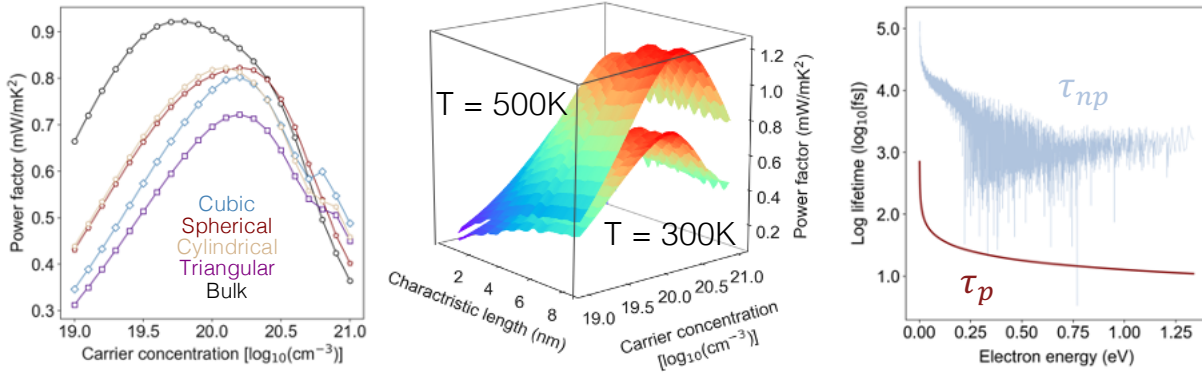


Figure 2: (left) The variation in power factor with carrier concentration for pores with different shapes. The power factor in bulk Si is marked with open circle in black. The spherical pores show the best performance with power factor as high as 89% of the bulk Si (marked with pentagon). The maximum power factor in porous structure always happens in higher carrier concentration than the carrier concentration that the bulk Si shows the best performance. (middle) The variation in power factor with pores length and carrier concentration in cubic pores at 300K and 500K. (right) Electron-pore lifetime for extended cylindrical pores at 300K in plotted in blue. The characteristic length is 3.3 nm. The electron lifetime due to phonons is plotted in red. This is the dominant scattering term. For extended pores with low porosity the Seebeck is similar to the bulk and the electrical conductivity is $(1 - \phi)$ of the bulk counterpart.

bulk Si. This is a key insight for the design of thermoelectrics: If one is planning to engineer porous thermoelectrics to reduce phonon conduction, then one should also plan to increase the carrier concentration above the optimal level for the bulk semiconductor. Spherical and cylindrical pores show the best ability for recuperating PF among the different pore shapes examined here, followed by cubic, and then triangular prismatic pores. In the Si model the maximum power factor with these two types of pores (spherical and cylindrical) takes place at $1.6 \times 10^{20} \text{ cm}^{-3}$ carrier concentration and is about 89% of the maximum power factor in bulk Si. The maximum power factor of triangular pores is less than 78% of the bulk Si. At higher temperatures a less extreme increase in carrier concentration is needed to recuperate the PF, and the recovery is larger. As an example, the maximum power factor of spherical pores at 500K takes place at $2 \times 10^{20} \text{ cm}^{-3}$ carrier concentration and is about 92% of the maximum power factor in bulk Si that takes place at $1.6 \times 10^{20} \text{ cm}^{-3}$ carrier concentration.

The central panel in figure (2) shows the change in PF as a function of carrier concentration and characteristic length for cubic pores at 300 K and 500K. For the characteristic length above 3.5 nm the largest enhancement of PF happens at carrier concentration of $1.6 \times 10^{20} \text{ cm}^{-3}$ and $2.5 \times 10^{20} \text{ cm}^{-3}$ at 300K and 500K, respectively. For the smaller pores, the maximum achievable PF varies non-monotonically with size.

E. Effect of extended pores on electron lifetime

To complete the model of electron-pore interaction, we considered extended cylindrical with infinite length (system size) oriented along the (001) crystal axis (the z -direction is our reference system) in a P-doped silicon slab. The thermal and electrical properties of such porous Si films have been studied in ^{3,15}, usually with the assumption that electron scattering is the same as that in bulk Si.² The electron lifetime of P-doped Si with extended cylindrical pores with 10 nm radius (3.3 nm characteristic length) and 0.05 porosity at 300K is depicted in the right-hand panel of figure (2). This plot shows that electron-phonon scattering is dominant over the pore scattering by one to two orders of magnitude. The dramatic reduction in the rate of electron scattering from discrete to extended pores is due to the limited number of states that are available to accept scattered electrons. For the analytic expressions for the scattering matrix elements see section B of the SI. In extended pores, scattering is only possible into states with the same component of wave vector along the pore axis. This condition, combined with the isoenergetic constraint, reduces the scattering integral to an elliptical line, drastically reducing the number of states that can participate in scattering, and means that the extended pores cause no change in the electron momentum along the axis of the pores. This result strengthens the assumption made in prior works^{2,16} that extended pores do not change the electron lifetime and thus the Seebeck coefficient of 2D nanoporous Si is the same as the bulk Si and electrical conductivity and power factor in 2D porous Si are $(1 - \phi)$ of their bulk Si counterparts.

F. Lorenz number in nanoporous silicon

We finish the argument on the effect of pores on electrical coefficients by briefly discussing the electronic thermal conductivity (κ_e). The κ_e is related to κ_e by Wiedemann Franz law as $\kappa_e = LT\sigma$. Here L is the Lorenz number that conventionally varies from $2 \times \left(\frac{k_B}{e}\right)^2 \approx 1.48 \times 10^{-8} \left(\frac{V^2}{K^2}\right)$ up to $\frac{\pi^2}{3} \times \left(\frac{k_B}{e}\right)^2 \approx 2.44 \times 10^{-8} \left(\frac{V^2}{K^2}\right)$ for low carrier concentration and degenerate (free electron) limit,

respectively.¹⁷ Lorenz number is related to Δ_n through $L = \frac{1}{(eT)^2} (\Delta_2 - \Delta_1^2)$. Figure 3 shows the variation of Lorenz number with characteristic length and carrier population in porous Si with cylindrical pores at 500 K. The effect of pores is more pronounced at low carrier populations where increasing pores length from 2.5 nm to 15 nm lower the Lorenz number up to 20%. Although, electron thermal conductivity is most of the semiconductors is much less than lattice thermal conductivity, for more accurate predictions, it is needed to compute κ_e by modified value for Lorenz number in nanoporous films.

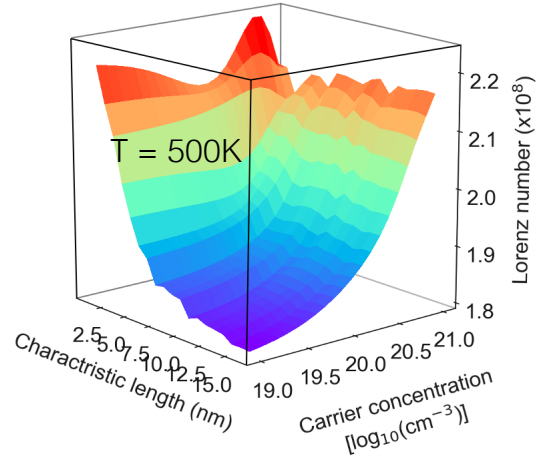


Figure 3: Variation of Lorenz number by carrier concentration and characteristic length of cylindrical pores at 500K.

III. CONCLUSION

To summarize, we have used a semiclassical model to elucidate detrimental effect of porosity on the electrical transport properties of thermoelectric, and to devise design strategies to mitigate them. We have shown that while extended pores have little effect on electron scattering, scattering from compact pores provides an electron filtering effect that increases the Seebeck coefficient. This effect becomes more pronounced for smaller pores but is relatively insensitive to the pore geometry. We find that to take full advantage of this effect to mitigate the degradation that pores cause to thermoelectric PF one should increase the carrier concentration above the optimal level for monolithic semiconductor. In this case one can recuperate as much as 90% of the lost thermoelectric PF because of the pores. While we have focused in particular a semiclassical model of P-doped Si, as this is a model that has been experimentally validated, the findings should be transferrable to other semiconductors systems both n- and p- type and with either direct or indirect band gaps. While there is much focus currently on designing porosity in thermoelectrics to dramatically impede phonon transport, the results presented here form a complementary design principle for optimizing the electrical transport properties in such devices.

APPENDIX A: DENSITY FUNCTIONAL THEORY CALCULATIONS

Density functional theory (DFT) was performed using the Vienna Ab initio Simulation Package (VASP)^{18–21} using generalized gradient approximation (GGA) with the Perdew-Burke-Erzerhof exchange correlation functional (PBE).²² Projector augmented wave (PAW) pseudopotentials is used represent the ion cores.^{23,24} The Kohm-Sham wave functions constructed using a planewave basis set with 700 eV energy cutoff. The Brillouin zone was sampled using 12×12×12 Monkhorst-Pack k-point grid.²⁵ The forces on the atoms minimized to better than 10^{-6} eV/Å to relax the Si primitive cell. The electronic band structure used to compute $D(E)$ on a 45×45×45 k-point grid. The group velocity was obtained from the conduction band curvature, $v = \frac{1}{\hbar} |\nabla_{\mathbf{k}} E|$ along the $\langle 100 \rangle$ directions on the Γ to X Brillouin zone path.

We have validated the transport model against a set of phosphorous-doped Si based thermoelectrics.¹² The electrical conductivity and Seebeck coefficient of bulk P-doped Si is shown in figure (1). The experimentally measured values are marked with open circles and the solid lines show the prediction of the semiclassical BTE model informed by the experimentally measured carrier population. The model gives a good fit to the experimental data across the full range of temperatures with a single tuning parameter

for electrical conductivity. For the Seebeck coefficient, A_0 , the model's single tuning parameter, cancels from the numerator and denominator of BTE equation of Seebeck (Equations (3-4)) giving a parameterless prediction for S . The model gives a good fit to the experimental data across the full range of temperatures with a single tuning parameter for electrical conductivity. The calculations were performed used a python package, *thermoelectric.py*, that we have made available for download through GitHub¹³.

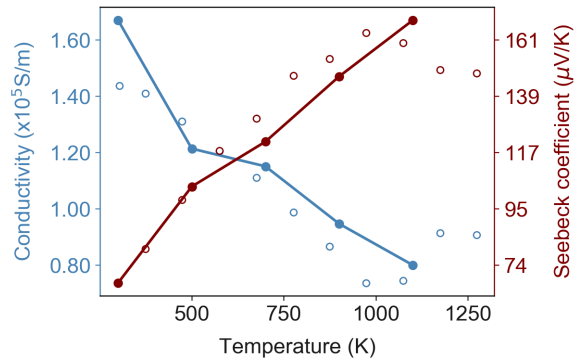


Figure A.1: The magnitude of electrical conductivity and Seebeck coefficient in phosphorous doped bulk silicon. The solid blue line shows the model prediction for electrical conductivity and the red line shows the prediction for the Seebeck coefficient. The experimentally measured σ and S are marked with open circles.

APPENDIX B: ELECTRON MATRIX ELEMENT OF PORES WITH DIFFERENT SHAPES

The electron matrix element shows the strength of the coupling between initial and final wavefunctions and the number of ways the transmission may happen. For the Bloch waves, matrix element relies on the shape of the scattering potential. Here we present the full expression for matrix element for pores with cubic, spherical, triangular and cylindrical shapes followed by matrix element for different shaped extended pores.

Cubic pore:

For cubic pores with finite lengths of l_x , l_y and l_z along x , y and z direction, respectively, electron matrix element describes as

$$M_{\mathbf{k}\mathbf{k}'} = 8U_0 \left(\frac{\sin\left(\frac{l_x q_x}{2}\right) \sin\left(\frac{l_y q_y}{2}\right) \sin\left(\frac{l_z q_z}{2}\right)}{q_x q_y q_z} \right). \quad (\text{B. 1})$$

In this equation, $\mathbf{q} = \mathbf{k} - \mathbf{k}'$, and $q_x = \mathbf{q} \cdot \hat{\mathbf{i}}$, $q_y = \mathbf{q} \cdot \hat{\mathbf{j}}$, $q_z = \mathbf{q} \cdot \hat{\mathbf{k}}$ are the projection of \mathbf{q} on cartesian axes.

Triangular prism pore

In prism with isosceles triangle base, matrix element defines as

$$M_{\mathbf{k}\mathbf{k}'} = -4U_0 l_y \left(\frac{l_x q_x - 2l_y q_y - 2l_x q_x e^{i\left(\frac{l_x q_x}{2} + l_y q_y\right)} + l_x q_x e^{i(l_x q_x)} + 2l_y q_y e^{i l_x q_x}}{l_x^2 q_x^3 - 4l_y^2 q_x q_y^2} \right) \left(\frac{\sin\left(\frac{l_z q_z}{2}\right)}{q_z} \right). \quad (\text{B. 2})$$

In this equation, l_x and l_y are the length and height of the triangle, respectively and l_z is the height of the prism.

Cylindrical pore

For cylindrical potential, we have

$$M_{\mathbf{k}\mathbf{k}'} = 4\pi r_o U_0 \left(\frac{J_\alpha(r_o q_r)}{q_r} \right) \left(\frac{\sin\left(\frac{l_z q_z}{2}\right)}{q_z} \right). \quad (\text{B. 3})$$

In this equation, $q_r = \sqrt{q_x^2 + q_y^2}$, r_o is the radius of the base circle, l_z is the height of the cylinder and J_α is the Bessel function of the first kind.

Spherical pore

Electron coupling matrix element for spherical potential defined as

$$M_{\mathbf{k}\mathbf{k}'} = \frac{4\pi U_0}{q^2} \left(\frac{1}{q} \sin(r_o q) - r_o \cos(r_o q) \right), \quad (\text{B. 4})$$

where, q is the magnitude of \mathbf{q} and r_o is the radius of pores.

Extended cubic pore

For cubic pores with infinite length (system size) along z the matrix element defines as

$$M_{\mathbf{k}\mathbf{k}'} = 4U_0 l_z \left(\frac{\sin\left(\frac{l_x q_x}{2}\right) \sin\left(\frac{l_y q_y}{2}\right)}{q_x q_y} \right) \delta(q_z). \quad (\text{B. 5})$$

Extended cylindrical pore

For the cylindrical pore with infinite height, we have

$$M_{\mathbf{k}\mathbf{k}'} = 2\pi r_o U_0 l_z \left(\frac{J_\alpha(r_o q_r)}{q_r} \right) \delta(q_z). \quad (\text{B. 6})$$

Extended isosceles triangular prism pore

For the isosceles triangular prism with infinite height matrix element describes as

$$M_{\mathbf{k}\mathbf{k}'} = -2U_0 l_y l_z \left(\frac{l_x q_x - 2l_y q_y - 2l_x q_x e^{i\left(\frac{l_x q_x}{2} + l_y q_y\right)} + l_x q_x e^{i(l_x q_x)} + 2l_y q_y e^{il_x q_x}}{l_x^2 q_x^3 - 4l_y^2 q_x q_y^2} \right) \delta(q_z). \quad (\text{B. 7})$$

¹ J. Tang, H.T. Wang, D.H. Lee, M. Fardy, Z. Huo, T.P. Russell, and P. Yang, Nano Lett. **10**, 4279 (2010).

² J.H. Lee, G.A. Galli, and J.C. Grossman, Nano Lett. **8**, 3750 (2008).

³ G. Romano and J.C. Grossman, Appl. Phys. Lett. **105**, (2014).

⁴ H. Lee, D. Vashaee, D.Z. Wang, M.S. Dresselhaus, Z.F. Ren, and G. Chen, J. Appl. Phys. **107**, 1 (2010).

⁵ G. Chen and D.M.E.G. Chen, *Nanoscale Energy Transport and Conversion: A Parallel Treatment of Electrons, Molecules, Phonons, and Photons* (Oxford University Press, 2005).

⁶ M. Lundstrom and C. Jeong, *Near-Equilibrium Transport* (WORLD SCIENTIFIC, 2011).

⁷ M. Lundstrom and C. Jeong, (2011).

- ⁸ A.J. Minnich, H. Lee, X.W. Wang, G. Joshi, M.S. Dresselhaus, Z.F. Ren, G. Chen, and D. Vashaee, 1 (2009).
- ⁹ H.R. Shanks, P.D. Maycock, P.H. Siddles, and G.C. Danielson, Phys. Rev. **130**, 1743 (1963).
- ¹⁰ J.R. Harter, S.A. Hosseini, T.S. Palmer, and P.A. Greaney, Int. J. Heat Mass Transf. **144**, 118595 (2019).
- ¹¹ S.M. Sze and K.K. Ng, *Physics of Semiconductor Devices* (John Wiley & Sons, 2006).
- ¹² S.A. Hosseini, D. Coleman, S. Bux, L. Mangolini, and P.A. Greaney, Manuscr. Submitt. Publ. (2020).
- ¹³ A. Hosseini, AriaHosseini/Thermoelectric.Py Thermoelectr. (Version v1.0) (2019).
- ¹⁴ L.C. Burton, J. Appl. Phys. **47**, 1189 (1976).
- ¹⁵ L. de Sousa Oliveira and N. Neophytou, Phys. Rev. B **100**, 35409 (2019).
- ¹⁶ J.H. Lee and J.C. Grossman, Appl. Phys. Lett. **95**, 93 (2009).
- ¹⁷ H.S. Kim, Z.M. Gibbs, Y. Tang, H. Wang, and G.J. Snyder, APL Mater. **3**, 1 (2015).
- ¹⁸ G. Kresse and J. Hafner, Phys. Rev. B **47**, 558 (1993).
- ¹⁹ G. Kresse and J. Hafner, Phys. Rev. B **49**, 14251 (1994).
- ²⁰ G. Kresse and J. Furthmüller, Comput. Mater. Sci. (1996).
- ²¹ G. Kresse and J. Furthmüller, Phys. Rev. B **54**, 11169 (1996).
- ²² J.P. Perdew, K. Burke, and M. Ernzerhof, Phys. Rev. Lett. **77**, 3865 (1996).
- ²³ P.E. Blöchl, Phys. Rev. B **50**, 17953 (1994).
- ²⁴ G. Kresse and D. Joubert, Phys. Rev. B **59**, 1758 (1999).
- ²⁵ H.J. Monkhorst and J.D. Pack, Phys. Rev. B **13**, 5188 (1976).